24th INTERNATIONAL CONGRESS ON SOUND AND VIBRATION
23–27 July 2017, London

ICSV24
23-27JULY 2017
LONDON CALLING

COMPOSITIONAL INHOMOGENEITIES AS A SOURCE OF INDIRECT COMBUSTION NOISE: PHYSICAL MECHANISMS AND FUEL EFFECTS

Matthias Ihme, Jeffrey O'Brien and Jeonglae Kim
Stanford University, Department of Mechanical Engineering, Stanford, USA
email: mihme@stanford.edu

Indirect combustion noise has been recognized as a main mechanism of engine-core noise in aviation gas-turbines. This noise mechanism is commonly associated with the distortion of temperature inhomogeneities and vortical structures that generate excess noise as they interact with mean-flow gradients. Recently, a new indirect noise-source mechanism was identified that arises from the interaction of mixture inhomogeneities and associated variations in the Gibbs free energy with the mean-flow gradients in the nozzle. By employing different levels of model fidelity in representing combustion noise, this work examines relative contributions of different noise source mechanisms, and the model fidelity that is necessary to accurately describe their relevant physical processes. For this, idealized one-dimensional compact and non-compact nozzle-analysis is performed, which is augmented by multidimensional transient flow-field calculations considering the linearized Euler equations. It is shown that the non-compact nozzle theory is necessary to accurately capture phase-cancellation effects between entropy and composition noise, and the linearized Euler formulation is required to account for complex mode shapes of the perturbations exiting the combustor and entering the downstream nozzle.
Keywords:

1. Introduction

In the quest to meet anticipated growth in air traffic, satisfy increasingly stringent efficiency requirements, and minimize pollutant emissions, significant efforts have been made to advance aircraft propulsion systems. In particular, advanced combustion concepts, such as lean premixed combustion, multi-point direct injection, and the operation at higher pressure ratios and increased power densities have been considered. However, these combustion concepts are often accompanied by the undesired effects of augmented combustion noise, incomplete combustion and reduced flame stability due to shortened residence time. Of particular concern to this work, combustion noise has been identified as a source of growing concern at low-power engine conditions, during landing and approach and in auxiliary power units [1].

Multiple noise-source mechanisms attributable to unsteady combustion in the engine core have been identified [2–4]. The first one is *direct combustion noise*, which describes the pressure fluctuations generated inside the combustion chamber caused by the unsteady heat-release of a turbulent flame [5]. These fluctuations radiate downstream through the engine core and are characterized by a broadband spectrum with peak-frequencies below approximately 500 Hz. The second core-noise mechanism is *indirect combustion noise*, which is generated by the convection and distortion of combustion-generated unsteady vortical, mixture composition, and temperature structures as they propagate from the combustor to the exhaust nozzle [6]. Through the interaction with mean-flow

and pressure gradients in the turbine and nozzle, these convective entropy, vorticity, and compositional modes are converted into pressure fluctuations that propagate to the far-field. An additional noise source, which is often not considered, arises from the *noise modulation* of the jet-exhaust by mean-flow deformation and flow-field inhomogeneities that are induced by combustion and unsteady flow-field effects from the engine core [4]. The relative contributions of different noise-source mechanisms arising from the engine core are strongly dependent on engine type, operating conditions, and interaction with other noise-source mechanisms.

Over recent years, significant progress has been made on the theoretical analysis and mathematical modeling of combustion noise. While acoustic analogies are most common for the characterization of direct combustion noise and jet-exhaust noise, different approaches have been pursued for analyzing indirect combustion noise. Perhaps most popular are low-order models for the evaluation of the indirect noise generated in nozzles and turbomachinery, which include the compact nozzle theory [6, 7], the effective nozzle length method [8], expansion methods [9], and non-linear analyses [10].

The objective of this work is to examine the current prediction capability for indirect combustion noise using different levels of model fidelity. Specifically, applying increasing levels of physical fidelity, we consider the compact nozzle theory [6], the expansion method [9, 11], and the linearized Euler formulation. The compact nozzle theory is valid in the limit of small Helmholtz numbers, $\mathrm{He} = fL/c \ll 1$ (where f is the frequency, L is the characteristic nozzle length, and c is the speed of sound at the nozzle inlet), and perturbations are assumed to propagate quasi-steadily through the nozzle. The expansion method relaxes this assumption by considering the nozzle to be non-compact, accounting for finite frequency effects. Both methods rely on a quasi one-dimensional flow representation. In order to relax this assumption, we lastly introduces a linearized Euler formulation in which the unsteady, two-dimensional, axisymmetric linearized Euler equations (LEE) are solved subject to a prescribed base flow.

These models are applied to predict the total combustion noise emitted from a gas-turbine model combustor that was experimentally investigated at the German Aerospace Agency [12]. To this end, large-eddy simulations (LES) are performed to obtain an accurate representation of the turbulent reacting flow-field inside the combustion chamber.

2. Experimental Configurations and Unsteady Combustor Simulations

Experimental Configurations The combustor geometry that is considered in this study is a dual-swirl gas turbine model combustor, which was designed to feature a flowfield and reaction zone representative of an aircraft engine combustor. The air flow is driven through a dual-swirl nozzle that produces a swirling inner airflow and a concentrically swirling annular outer airflow. Positioned between the two swirlers are 72 circularly-arranged capillary channels that inject methane gas into the chamber. The high degree of swirling flow and inner and outer shear layers allow the combustion zone to nearly resemble the conditions found in full-scale liquid fuel aero-engines. The flame is contained within a cylindrical combustion chamber with a diameter of 100 mm and a height of 113 mm. Downstream of the combustion chamber, the flow is strongly accelerated through a converging-diverging nozzle structure with a throat diameter of 7.5 mm which chokes the flow. Downstream of the nozzle lies an exhaust duct 1 m in length and 100 mm in diameter, which contains various acoustic probes positioned for the analysis of the acoustic sound field emitted by the combustion system.

Large-eddy Simulation of Turbulent Flow Field Large-eddy simulations are performed using the code CharLES, developed by Cascade Technologies. The computational domain was truncated upstream of the plenum section, and air is supplied at a constant mass flow rate over the plenum cross section. Fuel was supplied through the annular fuel injector at the inlet of the combustion chamber. A characteristic-but-reflecting inflow boundary condition was chosen for both the fuel and air inflow boundaries, with constant inflow temperature of 300 K and mass flow rates of 0.4 g/s and 7.56 g/s,

respectively. The burner is operated at an elevated pressure of 2.42 bar. The simulation included a portion of the downstream nozzle and exhaust tube, which was truncated 450 mm from the nozzle edge. This simplification did not affect the flow-field inside the combustor. The computational mesh consisted of approximately 70 million control volumes.

The turbulent combustion was modeled using the flamelet-progress variable (FPV) model. A lookup table was generated based on strained methane-air flamelets, which returned the reaction progress rate as a function of mixture composition and provided a closure for the equation of state. A constant timestep of 90 ns was chosen. The calculation was started from a cold, nearly stagnant pure air state, and the flame was ignited by injecting a negligible quantity of progress variable at the fuel inflow boundary for a short time to allow the reaction to take hold. The calculation was run for 120 ms until probe data indicated the flow had reached a steady state, and statistics were then collected for 100 ms, corresponding to two flow through times (excluding the diffusor) or 12.5 cycles of the lowest-frequency acoustic mode.

Statistical results from the LES-calculations are presented in Figure 1, showing axial velocity, temperature, and mixture fraction. Overlaid over Figure 1(a) are PIV-velocity measurements to provide a quantitative comparison between the simulation and experiment. It can be seen that the qualitative features of the flow, including a strong inner recirculation zone and an annular outer recirculation zone, are well captured by the simulation. Quantitatively, there are some discrepancies between the experimental and numerical results, including an under-prediction of the initial shear layer intensity. While some of these differences may be attributable to modeling errors or insufficient spatial resolution in the simulation, the geometry of the combustor posed several experimental challenges that may have contributed to this difference. In particular, optical access was compromised in the early shear layer due to the presence of the burner plate and strong reflections due to the annular glass chamber, which created blind spots at certain radial locations. With these caveats in mind, it is believed that the numerical prediction of the flow field is of appropriate quality for the purposes of investigating combustion acoustics. Statistical results for the temperature field, illustrated in Figure 1(b), show a V-shaped flame, which is stabilized by the inner and outer recirculation zones. The rapid mixing, shown in Figure 1(c), due to the strong swirl and precessing vortex core leads to a short flame.

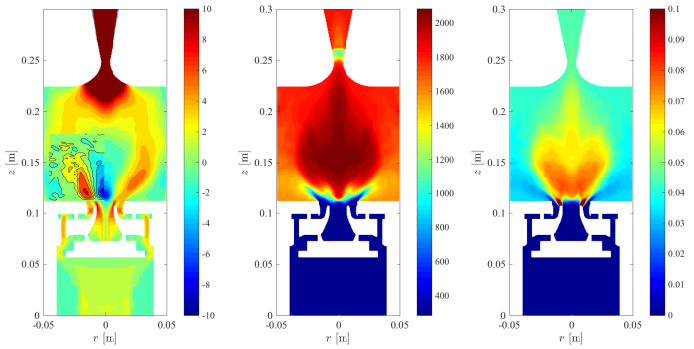

(a) Axial velocity (b) Temperature (c) Mixture fraction

Figure 1: Mean flow results for (a) axial velocity together with partial comparison against PIV-data (inlay), (b) temperature, and (c) mixture fraction.

Model Problem In this work, a hybrid model is considered to examine different levels of model fidelity in predicting the generation of indirect noise in a realistic combustor-nozzle configuration. The problem setup is schematically illustrated in Figure 2. In this configuration, the combustor LES provides mean-flow and perturbations as inflow conditions for the low-order nozzle simulation. This setup allows to obtain representative conditions about frequency,

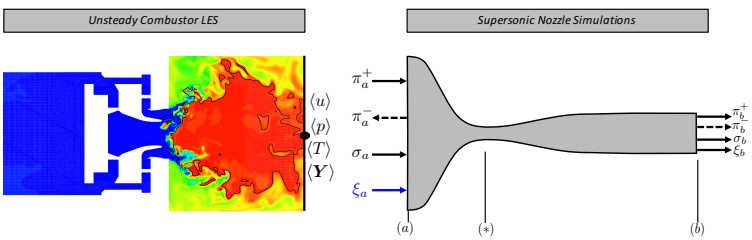

Figure 2: Schematic of hybrid model problem consisting of unsteady combustor LES and reduced-order model of the nozzle flow.

mode shape, and perturbation amplitude for velocity, pressure, temperature, and mixture composition. The nozzle is represented by a converging/diverging supersonic nozzle that is fully expanded, and the nozzle geometry in this study follows the linear-velocity profile nozzle by Duran & Moreau [9].

The length of the nozzle is $L = 1$ m, the throat diameter is $d^* = 9.3$ mm, and the inlet and exit diameters are, respectively, $d_a = 60$ mm and $d_b = 10.11$ mm. The mean flow-conditions at the combustor exit, entering the nozzle, are obtained from the LES and given as: $\langle Z \rangle_a = 0.051$, $\langle T \rangle_a = 1892$ K, $\langle p \rangle_a = 242$ kPa, and $\mathrm{M}_a = 0.05$, where Z is the mixture fraction, T is the temperature, p is the pressure, M is the Mach number, and $\langle \cdot \rangle$ is the spatio-temporal averaging operator. Using isentropic nozzle relations for a supersonic nozzle, the nozzle exit conditions for the mean-flow are evaluated as: $\langle Z \rangle_b = 0.051$, $\langle T \rangle_b = 1305$ K, $\langle p \rangle_b = 65.9$ kPa, and $\mathrm{M}_b = 1.5$.

3. Mathematical Model

Compact Nozzle Theory Marbel & Candel [6] employed compact nozzle theory to derive transfer functions relating acoustic and entropy perturbations at the nozzle inlet to resulting acoustic perturbations at the outlet. This theory was recently extended to account for the noise generation by compositional inhomogeneities [4], and subsequently applied to sub- and supersonic nozzle flows [13]. The compact nozzle theory is derived by applying jump conditions for normalized mass flow rate $I_{\dot{m}} = \dot{m}'/\dot{m}$, total sensible enthalpy $I_{h_t} = h_t'/h_t$, entropy $I_s = s'/c_p$, and mixture fraction $I_Z = Z'$ across the nozzle. For a choked supersonic nozzle flow, an additional condition at the sonic point is require to constrain all characteristic quantities. With this, transfer functions for the supersonic nozzle in the limit of $\mathrm{He} \to 0$ can be derived [4, 13], which are conveniently expressed in the characteristic form for the downstream and upstream acoustic waves, advected entropy perturbations, and compositional fluctuations, $\pi^{\pm} = \left(p'/\gamma\overline{p} \pm u'/\overline{c}\right)/2$, $\sigma = s'/c_p$, and $\xi = Z'$. The transfer function for the composition noise,

$$\pi_b^+/\xi_a = \frac{1}{2(\gamma-1)}\left[-\Psi_b + \frac{2+(\gamma-1)\mathrm{M}_b}{2+(\gamma-1)\mathrm{M}_a}\Psi_a\right], \tag{1}$$

introduces the chemical potential function, $\Psi = \frac{1}{c_p T}\sum_{i=1}^{N_s}\frac{\mu_i}{W_i}\frac{dY_i}{dZ}$, in which the chemical potential is evaluated from CHEMKIN-libraries.

Finite Nozzle Theory To account for the effects of finite frequency and nozzle geometry on the acoustic transmission, finite nozzle theory is employed [9, 11]. This model is derived by linearizing the governing equations, assuming a one-dimensional flow through the nozzle, and expressing the resulting set of equations in terms of the invariant vector $\boldsymbol{q} = (I_{\dot{m}}, I_{h_t}, I_s, I_Z)^{\mathsf{T}}$. After non-dimensionalizing time with frequency, $t = \tau/f$, velocity with speed of sound at the nozzle inlet $u = \widetilde{u}c_a$, and the axial coordinate with the nozzle length, $x = \eta L$, the following system of coupled linear, variable coefficient differential equations are obtained: $\mathrm{He}\partial_\tau \boldsymbol{q} = \mathbf{A}(\eta)\partial_\eta \boldsymbol{q}$, where $\mathbf{A}(\eta)$ is a matrix [11]. Integrating this equation with appropriate boundary conditions enables the calculation of the nozzle transfer function for finite perturbation frequencies.

Linearized Euler Equations Flow variables of the compressible Euler equations for a multicomponent mixture with a frozen chemistry are decomposed into a time-stationary base state (denoted by an overbar) and fluctuations around the base state (denoted by a prime) as $q = \overline{q} + q'$. Substituting the decomposed variables and collecting the first-order terms of the fluctuating quantities, the linearized Euler equations are obtained as

$$\partial_t s' + \overline{\boldsymbol{u}}\cdot\boldsymbol{\nabla}s' + \boldsymbol{u}'\cdot\boldsymbol{\nabla}\overline{s} = 0, \tag{2a}$$

$$\partial_t \boldsymbol{u}' + \overline{\boldsymbol{u}}\cdot\boldsymbol{\nabla}\boldsymbol{u}' + \boldsymbol{u}'\cdot\boldsymbol{\nabla}\overline{\boldsymbol{u}} + \left(p'/\gamma\overline{p} - s'/c_p - \Psi Z'\right)\overline{\boldsymbol{u}}\cdot\boldsymbol{\nabla}\overline{\boldsymbol{u}} + \boldsymbol{\nabla}p'/\overline{\rho} = \mathbf{0}, \tag{2b}$$

$$\partial_t p' + \overline{\boldsymbol{u}}\cdot\boldsymbol{\nabla}p' + \boldsymbol{u}'\cdot\boldsymbol{\nabla}\overline{p} + \gamma\left(\overline{p}\boldsymbol{\nabla}\cdot\boldsymbol{u}' + p'\boldsymbol{\nabla}\cdot\overline{\boldsymbol{u}}\right) = 0, \tag{2c}$$

$$\partial_t Z' + \overline{\boldsymbol{u}}\cdot\boldsymbol{\nabla}Z' + \boldsymbol{u}'\cdot\boldsymbol{\nabla}\overline{Z} = 0, \tag{2d}$$

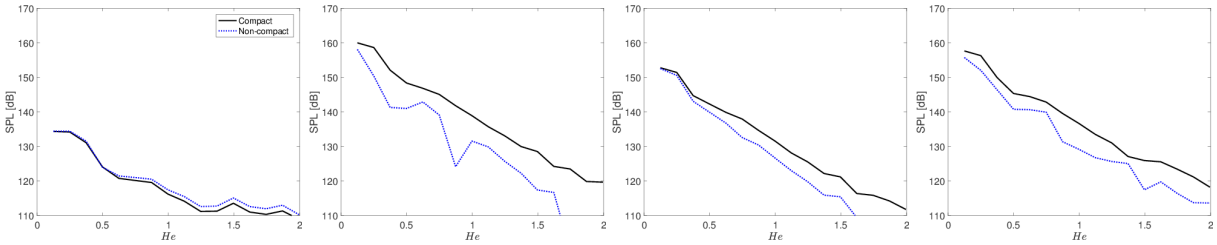

(a) Acoustic (b) Entropic (c) Compositional (d) Total

Figure 3: Sound pressure level predicted at the nozzle outlet due to (a) acoustic forcing, (b) entropic forcing (c) compositional forcing and (d) total sound as a function of dimensionless frequency He.

where s', $\boldsymbol{u}'$, p', and Z' are entropy, velocity, pressure, and mixture fraction fluctuations, respectively. The governing equations are non-dimensionalized using ambient quantities and time advanced in the physical space. Axisymmetry is explicitly enforced to the governing equations. The base state is prescribed in the same way as the quasi one-dimensional analyses. In addition, the mean radial velocity is computed to satisfy the mean continuity equation.

Spatial derivatives in the governing equations are transformed to curvilinear coordinates, and discretized using a standard fourth-order central finite difference scheme. The solution is time-advanced using the standard fourth-order Runge–Kutta method with a constant time-step size. For numerical stability, the standard eighth-order filter is applied at every time step in every direction.

4. Results

Quasi-1D Nozzle Results Applying the quasi-1D acoustic models described in Secs. 3 and 3 to the unsteady signals obtained from the combustor LES described in Sec. 2, the acoustic signature of the nozzle exhaust can be predicted. Figure 3 shows the predicted sound pressure levels (SPLs) attributable to each component of core noise, as well as the total amount of sound generated by all three mechanisms as a function of dimensionless frequency. It can be seen that both indirect core noise mechanisms (entropic and compositional fluctuations) produce significantly more downstream noise than the direct core noise mechanism. This is consistent with the prediction of [14] that, in flows with large accelerations typical of aviation engine applications, the indirect noise mechanism will dominate the direct noise mechanism.

Comparison between the acoustically compact and non-compact models indicates that indirect noise is attenuated at high frequencies while direct noise amplification becomes stronger with increasing Helmholtz number. This indicates that application of the simpler acoustically compact model will result in over-prediction of indirect core noise and under-prediction of direct noise and that the accuracy of the compact model decays much more rapidly for the convected scalar forcing than it does for the acoustic forcing. These findings are consistent with results reported earlier by [9] and [11].

Additionally, it can be seen that some degree of phase cancellation exists between the entropic and composition-induced noise, resulting in the total noise curve, shown in Fig. 3(d), lying below the entropic noise of Fig. 3(b). This behavior is explored in detail in Figure 4, which shows the time-domain forcing signal imposed at the nozzle exit and the corresponding acoustic signal emerging from the outlet. The entropy and composition signals should be highly correlated near the flame, since, given the very low Mach number inside the combustor, the gas temperature is determined largely by heat release which itself depends on the gas composition. Additionally, as the combustion products convect downstream toward the nozzle inlet, this relationship between T and Z is preserved since the scalars are modeled with the same diffusivity, so differences in these fields are attributable only to very weak compressibility effects or incomplete combustion. Accordingly, the entropy and composition fluctuations at the nozzle inlet, shown in Figures 4(b) and 4(c), are quite similar. The

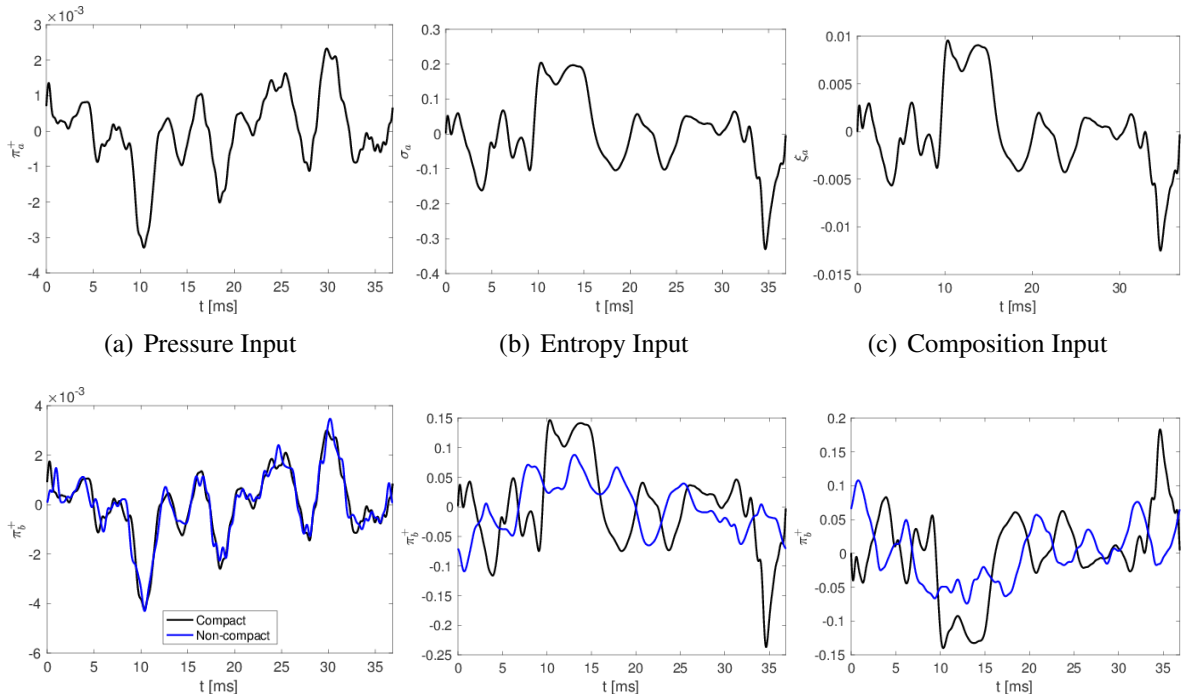

(a) Pressure Input (b) Entropy Input (c) Composition Input

(d) Direct Noise (e) Entropy Noise (f) Composition Noise

Figure 4: Non-dimensional inlet signals corresponding to (a) direct noise, (b) entropy fluctuations and (c) compositional fluctuations and (d-f) the corresponding acoustic response at the nozzle outlet.

transfer functions of these two mechanisms, however, produce acoustic fluctuations that are 180° out of phase, such that peaks in entropy-noise correspond to troughs in composition-noise and vice versa as seen in Figs. 4(e) and 4(f). This, in turn leads to destructive interference in the total sound produced and explains why the entropic component of the downstream sound (Fig. 3(b)) is at most frequencies larger than the total sound produced (Fig. 3(d)).

LEE Results To address the limitations of the quasi-1D model of compact and finite nozzle theory, multidimensional simulations using the linearized Euler formulation (see Eqs. 2) are performed. This formulation enables to investigate representative nozzle geometries and perturbations with spatial structure. In the following, we examine the effects of modal structure of incoming perturbations at the nozzle inlet on the acoustic transmission. For this, we consider three different cases: The first case consists of planar perturbations for incoming acoustic, entropy, and composition fluctuations, which serves as a verification against results from the quasi-1D nozzle theory (not shown here). The second case considers radial mode shape with a Gaussian distribution, which assumes that all perturbations are generated in the combustor core region. For the last case, a radial structure is extracted from a POD analysis performed at the combustor exit, and the most energetic mode for each perturbation is prescribed at the nozzle inlet. Incoming fluctuations have a single frequency $f = 1750$ Hz, corresponding to a Helmholtz number of $\mathrm{He} = 2$.

Simulation results are presented in Fig. 5, in which the magnitudes of corresponding upstream perturbations are used for normalization. Figure 5(a) shows the downstream-propagating acoustic waves, normalized by the nozzle-upstream forcing with Gaussian mode shape, and Fig. 5(d) corresponds to perturbations that are reconstructed from POD-analysis. These quantitative results show an axial distortion of the modal structure, and an increase in the wavelength as a result of the acceleration of perturbations through the nozzle.

Figure 6 shows time histories of cross-sectionally averaged outgoing acoustic waves, which are normalized by the nozzle-upstream perturbations with different modal shapes. It can be seen that the direct noise (shown in the left panel) is not affected appreciably by the modal shape of the upstream

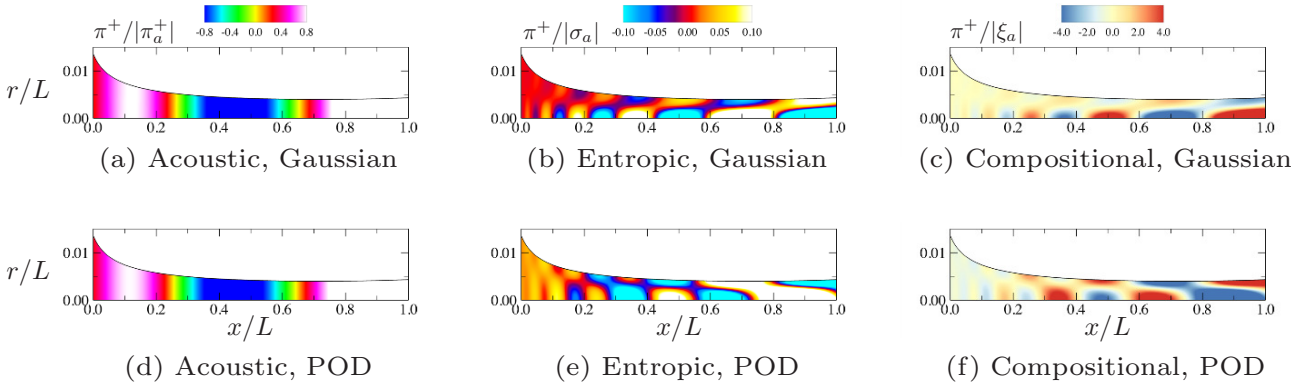

Figure 5: Instantaneous contours of normalized downstream-propagating acoustic waves. Top row, Gaussian distribution in the radial direction; bottom, mode shape of the most energetic POD mode. Simulations are performed at a constant Helmholtz number of $\mathrm{He} = 2$.

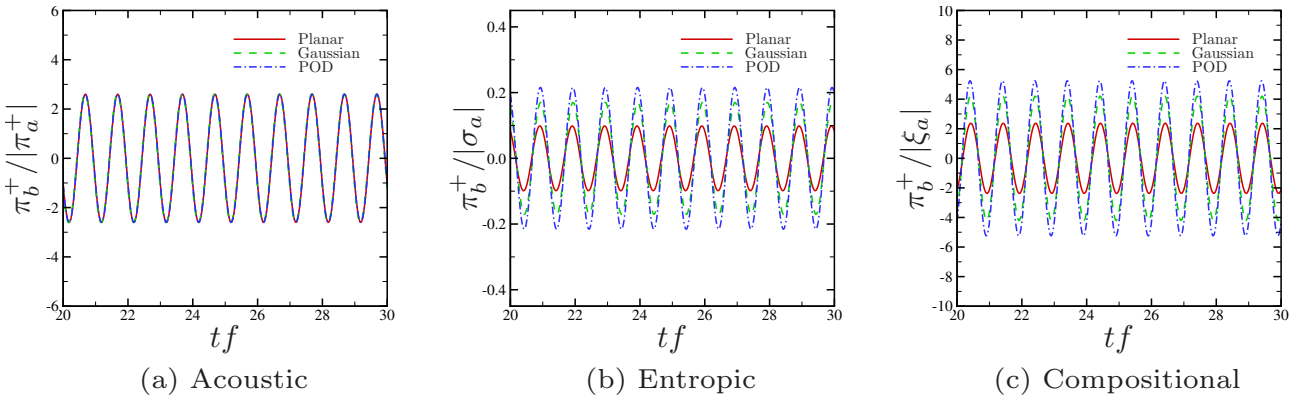

Figure 6: Normalized acoustic amplitudes at the nozzle outlet for (a) acoustic, (b) entropic, and (c) compositional perturbations.

pressure forcing. This can be explained by the initial propagation of the acoustic wave in the nozzle-inlet section. In contrast, appreciable differences in the pressure field are observed for the entropy and compositional noise, which is seen from Figs. 5 and 6. Depending on the mode shape and the frequency of the upstream perturbations, the magnitude of the transfer function was found to change significantly. This in turn indicates that the spatial mode shape requires consideration in accurately predicting combustion noise.

5. Conclusions

In this study, the generation and transmission of combustion noise in a supersonic nozzle is examined by employing different levels of model fidelity. The effects of finite perturbation frequencies, non-compact nozzle geometry, and mode shapes of the perturbations on the noise generation are investigated. To account for representative flow conditions, mean flows and nozzle perturbations are extracted from compressible LES of a dual-swirl gas-turbine combustor that was experimentally investigated at DLR. From the present study, the following conclusions can be drawn:

- Indirect combustion noise arising from entropy and composition noise was found to be the main noise-source contributor. Direct combustion noise was found to be approximately 10 dB lower than indirect combustion noise.
- Phase cancellation between entropy noise and composition noise results in overall reduction of the indirect noise. Non-compact nozzle theory or LEE is required to accurately capture frequency-dependent phase-shifts.

- Analysis of the flow-field at the combustor exist showed that perturbations exiting the combustor and entering the nozzle are only inadequately represented by planar modes. POD-analysis can be used to extract correct modal shapes. The consideration of modal perturbations appreciably affect the transfer functions and noise generation at the nozzle exit. The linearized Euler formulation is necessary to account for these effects, which are difficult to incorporate into quasi-1D nozzle-flow theory.

Acknowledgments

Finanical support through NASA with award number NNX15AV04A is gratefully acknowledged. Resources supporting this work were provided by the NASA High-End Computing (HEC) Program through the NASA Advanced Supercomputing (NAS) Division at Ames Research Center.

References

1. Hultgren, L. S., (2011), *Core Noise: Implications of Emerging N+3 Designs and Acoustic Technology Needs*. Acoustics Technical Working Group.

2. Candel, S., Durox, D., Ducruix, S., Birbaud, A.-L., Noiray, N. and Schuller, T. Flame dynamics and combustion noise: progress and challenges, *Int. J. Aeroacoustics*, **8** (1-2), 1–56, (2009).

3. Dowling, A. P. and Mahmoudi, Y. Combustion noise, *Proc. Combust. Inst.*, **35**, 65–100, (2015).

4. Ihme, M. Combustion and engine-core noise, *Annu. Rev. Fluid Mech.*, **49**, 277–310, (2017).

5. Strahle, W. C. A review of combustion generated noise, *AIAA Paper 73-1023*, (1973).

6. Marble, F. E. and Candel, S. M. Acoustic disturbance from gas non-uniformities convected through a nozzle, *J. Sound Vib.*, **55** (2), 225–243, (1977).

7. Cumpsty, N. A. and Marble, F. E. Core noise from gas turbine exhausts, *J. Sound Vib.*, **54** (2), 297–309, (1977).

8. Stow, S. R., Dowling, A. P. and Hynes, T. P. Reflection of circumferential modes in a choked nozzle, *J. Fluid Mech.*, **467**, 215–239, (2002).

9. Duran, I. and Moreau, S. Solution of the quasi-one-dimensional linearized euler equations using flow invariants and the Magnus expansion, *J. Fluid Mech.*, **723**, 190–231, (2013).

10. Huet, M. and Giauque, A. A nonlinear model for indirect combustion noise through a compact nozzle, *J. Fluid Mech.*, **733**, 268–301, (2013).

11. Magri, L., O'Brien, J. and Ihme, M. Effects of nozzle Helmholtz number on indirect combustion by compositional perturbations, *Proceedings of ASME Turbo Expo 2017: Turbomachinery Technial Conference & Exposition*, Paper GT2017-63382, (2017).

12. Bake, F., Kings, N., Fischer, A. and Röhle, I. Indirect combustion noise: Investigations of noise generated by the acceleration of flow inhomogeneities, *Acta Acust. united Ac.*, **95**, 461–469, (2009).

13. Magri, L., O'Brien, J. and Ihme, M. Compositional inhomogeneities as a source of indirect combustion noise, *J. Fluid Mech.*, **799** (R4), 1–12, (2016).

14. Leyko, M., Nicoud, F. and Poinsot, T. Comparison of direct and indirect combustion noise mechanisms in a model combustor, *AIAA J.*, **47** (11), 2709–2716, (2009).